Journal of
Composites Science

MDPI

Article

Microstructure Evolution of Polyacrylonitrile-Based Fibers during Thermal Pre-Oxidation

Yue Sun [1,2], Yanxiang Wang [1,2,*], Lanzhong Wang [3,*], Yongbo Wang [1,2], Bohan Ding [1,2], Jinghe Guo [1,2], Shichao Dai [1,2] and Yuxia Wang [1,2]

1 Key Laboratory for Liquid-Solid Structural Evolution and Processing of Materials (Ministry of Education), State Key Laboratory of Crystal Materials, Shandong University, Jinan 250061, China; 15908091665@163.com (Y.S.); wyongbo1011@163.com (Y.W.); 202314123@mail.sdu.edu.cn (B.D.); 202334193@mail.sdu.edu.cn (J.G.); 202314121@mail.sdu.edu.cn (S.D.); 202334246@mail.sdu.edu.cn (Y.W.)
2 Carbon Fiber Engineering Research Center, School of Materials Science and Engineering, Shandong University, Jinan 250061, China
3 School of Foreign Languages and Literature, Shandong University, Jinan 250100, China
* Correspondence: wyx079@sdu.edu.cn (Y.W.); lan2726@mail.sdu.edu.cn (L.W.)

Abstract: In this work, pre-oxidized polyacrylonitrile fibers are treated with ultrasonic etching and solution etching to produce ultra-thin sections. The evolution of the fibers' microstructure in the pre-oxidation process is observed, and the transformation model of the microstructure of the pre-oxidized fibers is proposed. Scanning electron microscopy and high-resolution transmission electron microscopy were used to observe the microstructure changes of the fibers. Fourier transform infrared spectroscopy and X-ray diffraction were used to observe the chemical structure transformation and crystallization degree of the fibers in the pre-oxidation process. The results revealed that pre-oxidized fibers exhibited a smooth surface, while their interior consisted of fibrils. The longitudinal microfibrils were connected by the transverse microfibrils and amorphous regions. The fracture morphology of the fibers shifted from ductile to brittle, and the cross-section gradually became smoother. The linear molecular chain of PAN transformed into a ring structure as pre-oxidation progressed, subsequently leading to the cross-linking of this ring structure into an orderly trapezoidal configuration. The connection between the fibrils was enhanced, and the fiber structure became more compact and stable.

Keywords: polyacrylonitrile; pre-oxidized fiber; microstructure; carbon fiber

Citation: Sun, Y.; Wang, Y.; Wang, L.; Wang, Y.; Ding, B.; Guo, J.; Dai, S.; Wang, Y. Microstructure Evolution of Polyacrylonitrile-Based Fibers during Thermal Pre-Oxidation. *J. Compos. Sci.* **2024**, *8*, 198. https://doi.org/10.3390/jcs8060198

Academic Editors: Xiangfa Wu and Oksana Zholobko

Received: 29 April 2024
Revised: 16 May 2024
Accepted: 21 May 2024
Published: 23 May 2024

1. Introduction

Carbon fiber is a high-performance fiber with carbon content exceeding 90% [1,2]. Due to its high strength, high modulus, and lightweight properties, it is widely used in aerospace, military, automotive, construction, and sports industries [3–5]. Carbon fiber can be divided into pitch-based carbon fiber, polyacrylonitrile-based (PAN) carbon fiber, and bio-based carbon fiber [6,7], with polyacrylonitrile-based carbon fiber currently holding the largest market share [8]. This type of carbon fiber is made through processes such as precursor polymerization, pre-oxidation, low-/high-temperature carbonization, and graphitization [9,10]. Among these steps, pre-oxidation is considered a crucial link, which transforms the linear polymer chain into a stable trapezoidal structure [11,12].

The pre-oxidation process is characterized by lengthy time consumption, high energy costs, and irreversible chemical reactions. In addition, the results of pre-oxidation on the polymer precursor are further inherited in the subsequent carbonization and graphitization processes, ultimately affecting the mechanical properties of carbon fibers [13]. The pre-oxidation of polymer precursors can be conducted through a variety of methods, the most common of which is the gradient heating method [14]. In the pre-oxidation process,

the polymer precursor will undergo cyclization, dehydrogenation, oxidation, and intermolecular crosslinking reactions [15]. Dehydrogenation and cyclization are two important reactions and form a stable trapezoidal structure, which can resist high-temperature conditions in the subsequent carbonization and pyrolysis process. By pre-oxidation in an oxygen-containing environment, a polymer backbone containing oxygen-bearing groups can be generated, providing higher stability in the subsequent high-temperature carbonization process. The dehydrogenation reaction occurs after the oxidation reaction, with the introduction of oxygen and the removal of hydrogen in the form of water molecules. Dehydrogenation can occur both before and after cyclization. After cyclization, the nitrile group and adjacent functional groups form a stable trapezoidal polymer [16]. Therefore, there are complex chemical structural changes in the pre-oxidation process, and these complex changes can affect the microstructure of polyacrylonitrile fibers.

The performance of carbon fibers is largely determined by their microstructure, which includes crystal orientation, crystal structure, the skin–core structure, and graphitization [17]. The skin–core structure appears in the pre-oxidation process of precursor polymers, and refers to the uneven distribution of the fiber structure along the radial direction [18,19]. The structure of the fibrous cortex is denser and the core is looser. Many observations and studies have been conducted on the microstructure during the pre-oxidation process. Gao et al. treated the ultra-thin fiber slices via solution etching and analyzed the internal structure of the PAN precursor through high-resolution transmission electron microscopy (HRTEM), clarifying the formation and evolution mechanisms of the interconnected microfiber network and lateral lamellae of the PAN nascent fibers in the solidification process [20]. He et al. observed the microstructure of the polyacrylonitrile precursor fibers at different stages in the dry–wet spinning post-processing process. Through the scanning electron microscopy (SEM) observation of the surface topography, it was found that the fiber structure became denser with the processing process. An HRTEM observation of the ultra-thin section of the fibers indicated that there was a unique skin–core structure in PAN, and with further processing, the difference in skin–core structure decreased [21]. Lee et al. used the gradual etching method (from the surface to the inside) to study the relationship between the changes in the radial microstructure and mechanical properties of commercial PAN-based carbon fibers in the pre-oxidation process, and concluded that the pore diameter and crystal orientation were the main structural factors determining the mechanical properties of carbon fibers [9]. In recent years, there has been some progress in studying the microstructure of pre-oxidized fibers, but there is little information on the evolution of fibrils during pre-oxidation. Further research is needed on the evolution mechanisms of the microstructure of pre-oxidized fibers in various temperature zones.

In this study, the pre-oxidized fibers were prepared through gradient temperature pre-oxidation, and the fibers were treated via ultrasonic etching and solution etching ultra-thin sections. The evolution mechanism of the microstructure of the pre-oxidized fibers was examined using scanning electron microscopy (SEM), X-ray diffraction (XRD), high-resolution transmission electron microscopy (HRTEM), and Fourier transform infrared spectroscopy (FTIR). A new model for the evolution of the pre-oxidized fiber structure is proposed to enrich the structural theory of fibers.

2. Experimental

2.1. Samples and Preparation

PAN fiber was prepared via a dry-jet wet spinning process on a production line at Shandong University. PAN fiber was pre-oxidized via gradient heating in an air atmosphere within a pre-oxidation furnace, passing continuously through six temperature zones. The temperatures of the temperature zones were 240 °C, 245 °C, 250 °C, 260 °C, 270 °C, and 285 °C, respectively. The pre-oxidation time for each temperature zone was set to 8 min, and the zones were labeled PO1, PO2, PO3, PO4, PO5, and PO6. The ultrasonic etching process involved the following: first, the pre-oxidation fiber was cut with scissors and placed in a centrifuge tube, a specific concentration of dimethyl sulfoxide (DMSO) solution

was added, the centrifuge tube was placed in an ultrasonic cleaner, and the fiber was ultrasonically etched in hot water at 75 °C at an ultrasonic frequency of 40 kHz. After etching, the fiber was removed with a copper net, washed with deionized water at 75 °C, and air-dried naturally. The process of preparing ultrathin sections is as follows: Fiber microsegments were embedded in epoxy resin; after waiting for the resin to cure, the cured epoxy resin containing the fibers was cut using an ultra-thin slicer. Ultrathin sections with a thickness of 50 nm were prepared and deposited on a copper net with a carbon-supporting film. The ultrathin slices on the copper mesh were placed in a solution containing a specific concentration of DMSO and etched in a water bath at 75 °C.

2.2. Characterization

SEM (SU-70, Hitachi of Japan, Tokyo, Japan) was used to characterize the surface and cross-section of the pre-oxidized fiber. Gold spray was used to increase the conductivity of the sample before the test, and the test voltage was 5 kV. HRTEM (JEM-2100, JEOL Company of Japan, Tokyo, Japan) was used to characterize the pre-oxidized ultra-thin section sample after solution etching and depositing on the copper mesh; the internal morphology of the fiber was observed, and the test voltage was 200 kV. The pre-oxidized fibers were 'pulled off' with a fiber extensometer (XQ-1C, Donghua University of China, Shanghai, China) to observe the tensile morphology. During the test, a single fiber was clamped with a clamp at a distance of 20 mm and a tensile speed of 40 mm/min. FTIR (BRUKER TENSOR-37, BRUKER of Germany, Berlin, Germany) was used to determine the chemical structure of the pre-oxidized fiber. At room temperature, the sample was processed by a pressing method, and the test range was 4000–400 cm^{-1}. XRD (Rigaku D/max-RC, Rigaku Corporation of Japan, Tokyo, Japan) was used to characterize the crystal structure of the pre-oxidized fiber. The fiber was attached to the glass plate, and Ni-filtered/CuKα radiation sources were used to test at a voltage of 40 kV and a current of 50 mA, with the scanning range of 2θ set between 5 and 50°. The crystallinity X_c of the pre-oxidized fiber is usually calculated by the following formula [22]:

$$X_c = \frac{A_c}{A_c + A_a} \times 100\% \quad (1)$$

where A_c represents the area of the crystallization region and A_a represents the area of the amorphous region.

The grain size L_c of the pre-oxidized fiber is generally calculated by the following formula [23]:

$$L_c = \frac{K\lambda}{B\cos\theta} \quad (2)$$

where θ represents the Prague angle, B represents the half height near $2\theta \approx 16.9°$, λ is the incident wave wavelength of 0.1541 nm, and K = 0.89.

Fibers in the pre-oxidation stage are usually evaluated by the infrared conversion index to determine the content of cross-linked trapezoidal polymers in the pre-oxidation fibers [24]:

$$IR - Conversionindex = \frac{I_c}{I_c + I_n} \times 100\% \quad (3)$$

where I_c is the peak indensity of C=N at about 1590 cm^{-1}, and I_n is the peak intensity of C≡N at 2242 cm^{-1}.

3. Results and Discussion

3.1. Basic Structural Characterization of PAN Fibers

Figure 1a,b display typical infrared and XRD spectra of six pre-oxidized fibers within the 3250–1000cm^{-1} region across different temperature ranges. Figure 1a shows several typical functional group structures in the pre-oxidation process; 1600 cm^{-1} denotes the stretching vibration peak of C=N in cyclization PAN, and 2243 cm^{-1} denotes the stretching vibration peak of C≡N; 1365 cm^{-1}, 1452 cm^{-1}, and 2939 cm^{-1} correspond to the C-H

bending vibration peak in -CH, the C-H symmetric bending vibration peak in $-CH_2$, and the C-H symmetric extension vibration peak in $-CH_2$. The peaks at 1666 cm^{-1} and 1733 cm^{-1} denote the stretching vibration peaks of C=O [25–28]. During pre-oxidation, the peak intensity at C=N increased and the peak intensity at C≡N decreased with increasing temperature, indicating that the PAN linear molecular chain produced cyclized cross-links and gradually changed to a stable trapezoid structure. The peak strength of -CH increased and that of $-CH_2$ decreased, indicating that $-CH_2$ transformed to -CH and dehydrogenation occurred. In addition, the stretching vibration peak at C=O was continuously enhanced, indicating that the occurrence of the oxidation reaction was related to the formation of the ring-conjugated carbonyl structure.

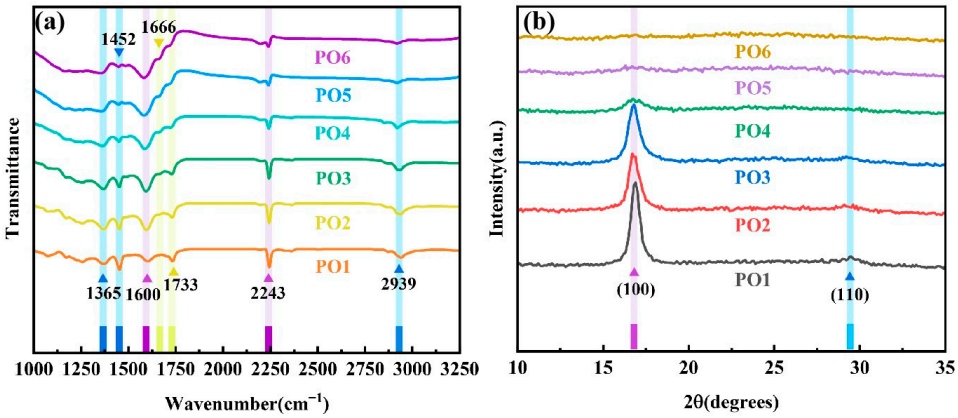

Figure 1. Basic structural characterization of pre-oxidized fibers: (**a**) FTIR spectra; (**b**) XRD patterns.

In Figure 1b, two distinct diffraction peaks at around $2\theta \approx 16.8^\circ$ and $2\theta \approx 29^\circ$ correspond to crystal planes (100) and (110), respectively [27]. As the temperature of the pre-oxidation heat treatment increased, the intensity of the two diffraction peaks continuously decreased, indicating that the degree of crystallization decreased and the crystal structure changed. When the temperature increased from 250 °C to 260 °C, the intensity of the crystal plane (100) decreased greatly, and the crystal structure obviously changed. Table 1 exhibits the crystallization parameters of the pre-oxidized fibers, showing that the crystallinity and grain size of the pre-oxidized fibers continuously decreased. This was due to the fact that—with the increase in temperature—the original crystal structure was destroyed during heating, the chemical structure inside the pre-oxidized fiber was changed, the PAN linear molecular chain was transformed into a cross-linked trapezoid structure, and a new sequential structure gradually formed.

Table 1. Crystallization parameters of pre-oxidized fibers.

Sample	PO1	PO2	PO3	PO4	PO5	PO6
B (°)	0.604	0.724	0.804	—	—	—
X_c (%)	68.69	67.13	65.72	—	—	—
L_c (nm)	23.75	19.82	17.84	—	—	—

The infrared conversion index of the pre-oxidized fiber, obtained from Figure 1a from the FTIR spectrum of the pre-oxidized fiber and Equation (3), is shown in Figure 2. The change in its value represents the transformation of the nitrile-based structure to the conjugated structure, that is, the cross-linked cyclization of the PAN linear molecular chain into a trapezoidal polymer. In the initial stage of pre-oxidation, the structural transformation was faster, and the infrared transformation index reached about 75% in the first four temperature regions of pre-oxidation. The magnitude of the transition subsequently decreased. In general, the polyacrylonitrile structure was mostly transformed into a cyclized

and cross-linked trapezoid structure at about 260 °C in the fourth temperature region of pre-oxidation.

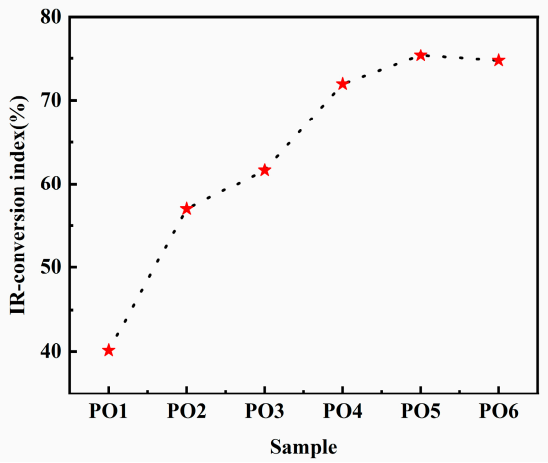

Figure 2. Infrared conversion index of pre-oxidized fibers.

3.2. SEM Surface Morphology of Pre-Oxidized Fibers

Figure 3a–f shows the surface SEM morphology of the pre-oxidized fibers. The surfaces of the pre-oxidized fibers in the first to sixth temperature zones were smooth, without obvious defects and grooves, and the diameters of the fibers from PO1 to PO6 were about 8 μm each.

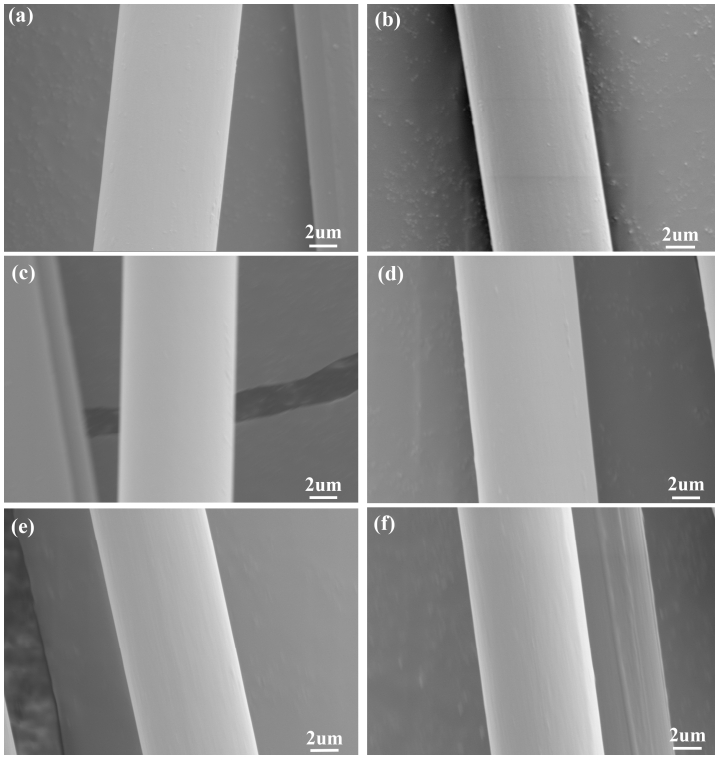

Figure 3. Surface morphology of pre-oxidized fibers: (**a**) PO1, (**b**) PO2, (**c**) PO3, (**d**) PO4, (**e**) PO5, and (**f**) PO6.

3.3. SEM Surface Morphology of Pre-Oxidized Fibers after Ultrasonic Etching

DMSO dissolved the fibers in two stages: swelling followed by dissolution. The DMSO solution first diffused into the interior of the fiber, causing its volume to increase and swell. Then, with the solvent increase, the interior began to dissolve. Figure 4 shows the SEM

surface morphology and partial cross-sectional morphology of the pre-oxidized fibers after ultrasonic etching in 98 wt% DMSO solution for 15 h; it shows the morphological changes of the pre-oxidized fibers after ultrasonic etching. Compared with the untreated fibers (Figure 3), the surface of the etched pre-oxidized fibers shows folds and the diameter is significantly larger, which is due to the chemical structural changes of PAN protofilaments after pre-oxidation, where the intermolecular force is weakened, and the solvent is diffused into the fiber interior. In the later stages of pre-oxidation, the cortex of the pre-oxidized fibers became relatively dense due to the oxidation and cyclization reactions between molecules. It was difficult for the solvent to diffuse into the fiber interior, resulting in less increase in the fiber diameter. Figure 4(a1–c1) show the cross-sectional morphology of the fiber in the three temperature zones before the pre-oxidation heat treatment. It could be seen that with the increase in the treatment temperature, the influence of the solvent on the inside of the fiber gradually decreased, indicating that the fiber became more compact. The fracture morphology gradually shifted from ductile to brittle, and the fracture surface gradually flattened. After the fourth temperature zone, the fibers became denser, and almost no fibers were broken.

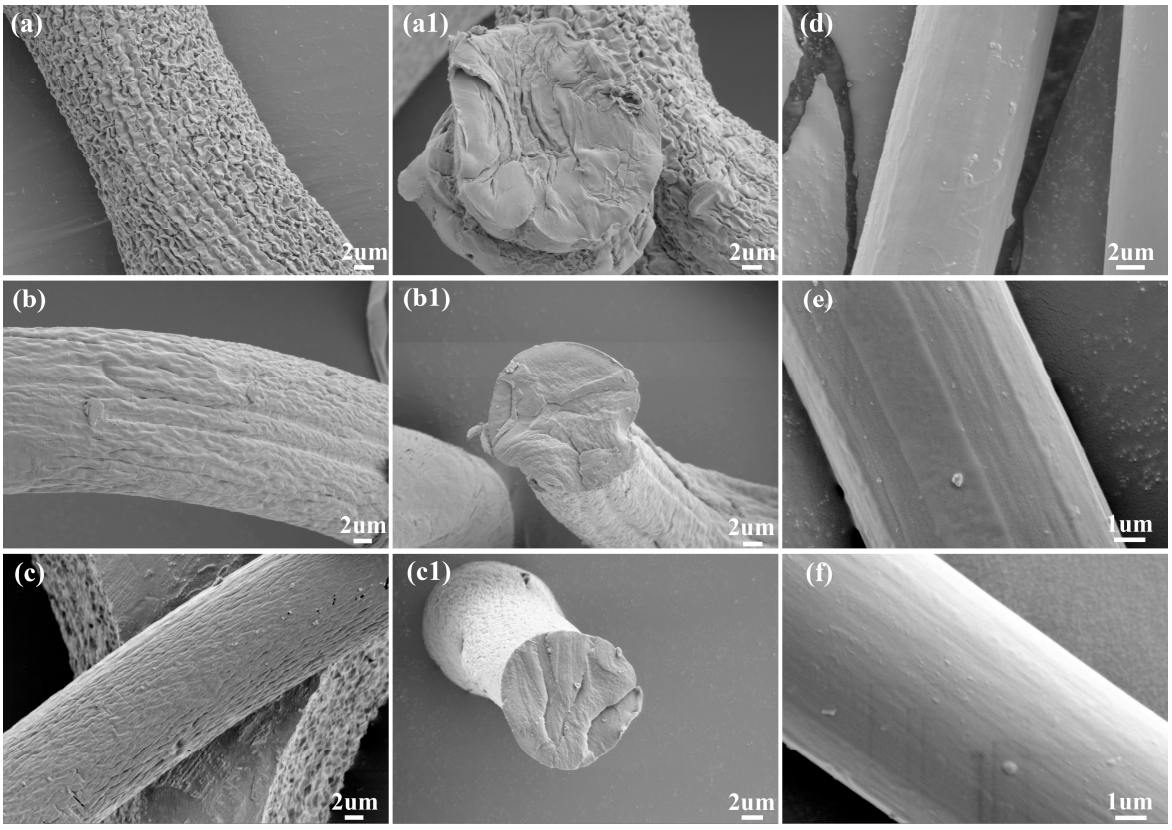

Figure 4. SEM morphology of pre-oxidized fibers after ultrasonic etching in 98wt% DMSO solution for 15 h: (**a**) PO1, (**b**) PO2, (**c**) PO3, (**d**) PO4, (**e**) PO5, (**f**) PO6; (**a1–c1**) the cross-sectional morphology of PO1, PO2, and PO3.

Figure 4 also shows that pre-oxidation increased the corrosion resistance of the fibers. When the pre-oxidized fiber was in the fourth temperature zone, the corrosion resistance of the fiber was significantly enhanced, and it was difficult for the solvent to diffuse into the fiber interior, indicating the formation of a large number of trapezoidal cross-linked structures at this stage; the pre-oxidized fiber formed a dense surface.

3.4. SEM Surface Morphology of the Cross-Sections of Tensile-Fractured Pre-Oxidized Fibers

Figure 5 shows the cross-sectional morphology of the pre-oxidized fibers in the first to the fourth temperature zones, broken by stretching. As shown in Figure 5(a,a1), when the pre-oxidized fibers in the first temperature zone were 'pulled off', many longitudinal lamellar microfibers extended along the stretching direction, and a large number of microfibers on the surface and in the inner layers of the fibers were extended, while some small transverse microfibers could also be observed. In Figure 5(b,b1), it could be observed that there was also a large number of lamellar structures when the pre-oxidized fibers in the second temperature zone were 'pulled off'. The extension length of microfibers in both the fiber cortex and inner layer was similar but shorter than that in the first temperature zone. This indicated that the connections between microfibers gradually strengthened with the increase in the pre-oxidation heat treatment temperature. As shown in Figure 5(c,c1), the pre-oxidized fibers in the third temperature zone became denser, and almost no lamellar microfibers in the fiber cortex were stretched or extended when the fiber was 'pulled off'; only the relatively weak microfibers in the inner layer of the fiber extended when stretched. Figure 5(d,d1) display the tensile fracture morphology of the pre-oxidized fiber in the fourth temperature zone. At this time, the pre-oxidation temperature was already high, the microfibers in the outer and inner layers of the fiber were (almost) neither stretched nor extended, and the connections between the microfibers had become very dense. It could be seen that the fracture morphology of the fiber changes from ductile to brittle, as well as the cross-section, became relatively flat.

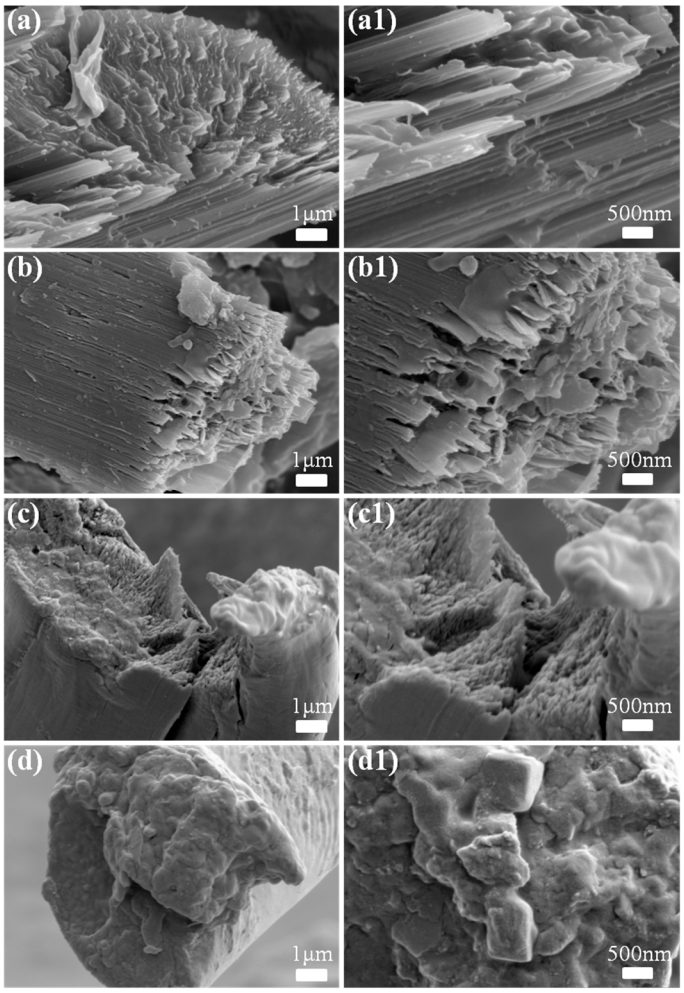

Figure 5. Surface morphology of the cross-sections of tensile-fractured pre-oxidized fibers: (**a**–**d**) PO1–PO4 low magnification; (**a1**–**d1**) PO1–PO4 high magnification.

3.5. HRTEM Morphology of Pre-Oxidized Fiber Ultrathin Slices after Solution Etching

DMSO was an effective solvent for PAN. In order to observe a more subtle fibrillar structure, ultrathin fiber slices were etched with a DMSO solution. If the concentration of the DMSO solution was too low or the etching time was too short, the amorphous tissue of fiber could not be fully solved; if the concentration of the DMSO solution was too high or the etching time was too long, the copper mesh would fall off. After many experiments, it was determined that the best morphology was obtained by etching slices for 2 h with 92 wt% DMSO solution.

Figure 6 shows the HRTEM morphology of the ultra-thin section of the first to the third temperature zones of the pre-oxidized fiber after etching with 92 wt% DMSO solution for 2 h. Figure 6a–f present a low-magnification view of the section of the first to the sixth temperature zones, with the blue arrow denoting the fiber axis orientation; Figure 6(a1–f1) shows an enlarged view of the local area within the red wireframe in Figure 6a–f.

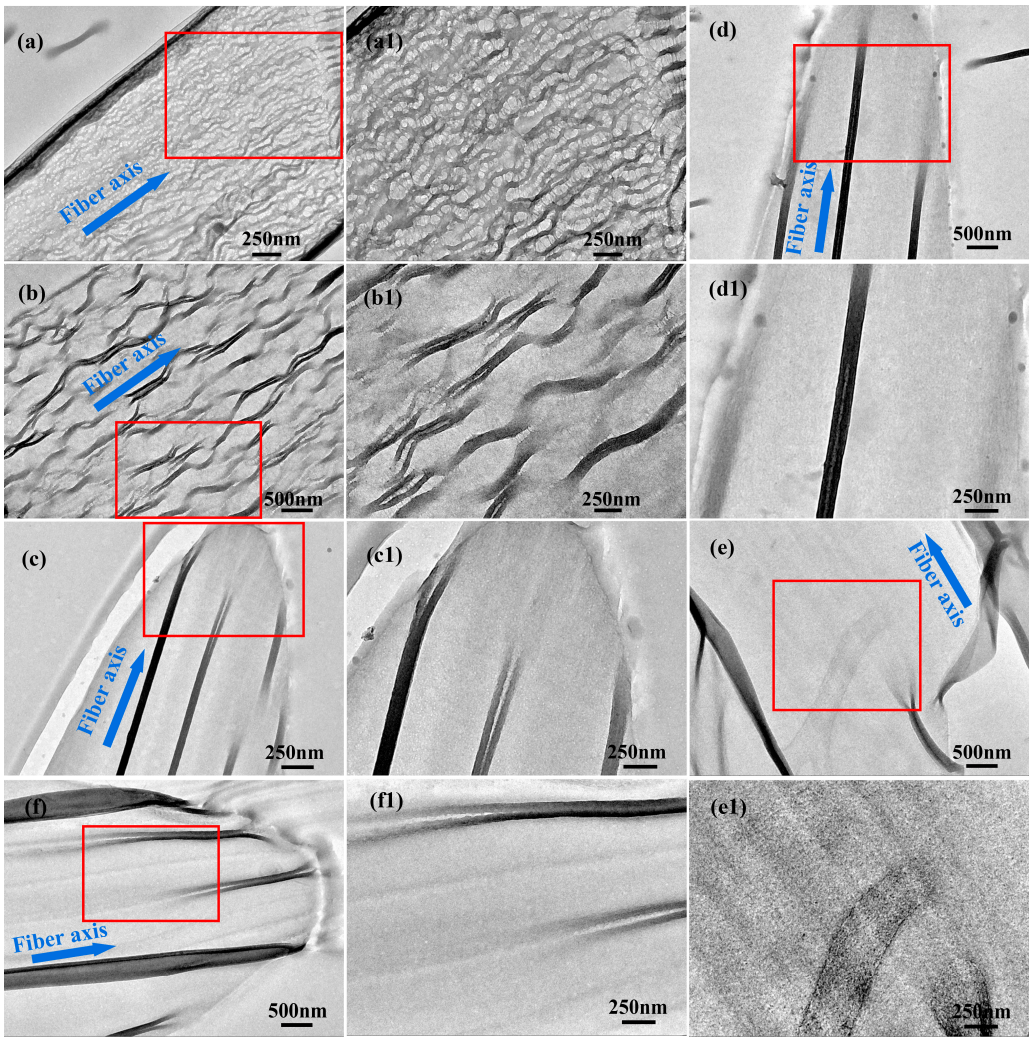

Figure 6. HRTEM morphologies of ultrathin sections of pre-oxidized fibers after solution etching: (**a**–**f**) PO1–PO6—low magnification, (**a1**–**f1**) PO1–PO6—high magnification.

As shown in Figure 6(a,a1), after the ultrathin section of the first temperature zone was etched, the amorphous tissue was fully dissolved, and uniformly arranged fibrils were separated, showing longitudinal microfibrils along the fiber axis with large sizes, 18–56 nm width, and transverse microfibrils perpendicular to the fiber axis with a small size, connected between longitudinal microfibrils. In the first temperature zone, almost all the amorphous tissue area was dissolved in the fiber section, and the fiber skeleton

was exposed. The inner part of the fiber was formed by microfibrils and amorphous tissue, and the transverse microfibrils and amorphous tissue served as bridges between the longitudinal microfibrils.

As shown in Figure 6(b,b1), after etching, the sections appeared as fibrillar structures, along the fiber axis and perpendicular to the fiber axis, and the width of the longitudinal microfibrils ranged from 25 to 108 nm. Compared with the longitudinal microfibrils, after dissolution and etching in the first temperature zone, thicker microfibrils appeared in the second temperature zone, which was related to the chemical reactions occurring during the pre-oxidation process.

As shown in Figure 6(c,c1), only part of the same section in PO3 was dissolved and etched, and the microfibril structure appeared in thinner areas of the section, which was caused by a further increase in the corrosion resistance of the fibers, and the microfibril width was measured to be 15–98 nm. There were only a few longitudinal microfibrils inside the section, the transverse microfibril structure could hardly be observed, and no obvious fibril skeleton appeared. This indicated that in the third temperature zone, the internal structure of the fiber began to show obvious differences, which was due to the higher degree of fiber pre-oxidation in this temperature zone. The chemical reactions facilitated the internal formation of more ring structures, and the fiber structure was more compact.

Figure 6(d,d1) show that compared with PO1-PO3, the dissolved tissue inside the fibers gradually decreased as the pre-oxidation proceeded. As shown in Figure 6(d1), the etched sections had a small number of microfibril structures along the fiber axis, with widths ranging from 46 to 78 nm. This was because, at this stage, a large number of ring structures were generated, PAN linear molecular chains were transformed into trapezoid-shaped structures, cross-linked cyclization occurred between molecules, and new sequential structures began to form inside the fiber, which enhanced the corrosion resistance.

As shown in Figure 6(e,e1), a few primitive fiber structures appeared in the fiber sections, and no dissolution occurred in most areas, indicating that the corrosion resistance of the fiber was further improved. It indicated that a very dense structure was formed inside the pre-oxidized fiber at this stage.

As shown in Figure 6(f,f1), slices of pre-oxidized fibers could hardly be dissolved by the DMSO solution, which was consistent with the structures of unetched slices, indicating that in the final stage of pre-oxidation, the pre-oxidized fibers underwent cross-linking and cyclization to form a compact and ordered trapezoid structure with strong resistance to solvent corrosion.

The analysis of the pre-oxidized fibers in different temperature zones showed that the amorphous region of the fiber section was dissolved during the dissolution etching process, and the transverse microfibrils and longitudinal microfibrils with good orientation were displayed inside the fiber. The longitudinal microfibrils were connected by the transverse microfibrils and the amorphous tissue as a bridge. With the increase in the pre-oxidation temperature, the area where the DMSO solution was dissolved gradually decreased, and the corrosion resistance of the fibers gradually increased.

3.6. Mechanical Strength of Pre-Oxidized Fibers

As shown in Figure 7 and Table 2, the tensile strength of the pre-oxidized fiber decreased continuously from the first to the sixth temperature zones. The tensile modulus decreased gradually. Elongation at the break increased continuously and decreased in the sixth temperature zone. During the pre-oxidation process, XRD and FTIR analyses indicated that with the pre-oxidation treatment temperature increase, the nitrile group changed into the conjugated group, and the molecular cohesion decreased, leading to a decrease in tensile strength and tensile modulus. However, the crystalline size of the fiber gradually decreased, and the amorphous area increased, resulting in enhanced fiber ductility and, therefore, increased elongation at break. When the fiber reached the sixth temperature zone, the rigidity increased and the elongation at break decreased.

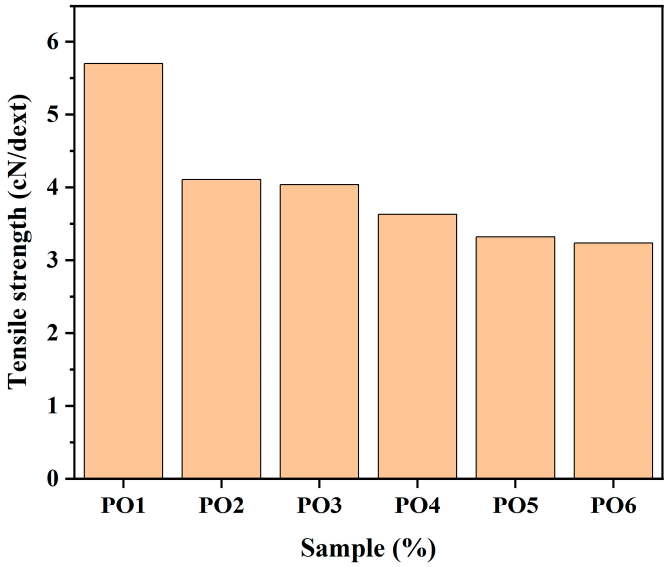

Figure 7. Tensile strengths of pre-oxidized fibers.

Table 2. Tensile moduli of pre-oxidized fibers.

Sample	PO1	PO2	PO3	PO4	PO5	PO6
Elongation at break (%)	12.76	14.38	15.73	16.03	16.05	12.74
AV [a] (cN/dtex)	6.20	6.14	5.98	4.64	4.62	4.56
CV [b] (%)	11.42	11.53	9.92	14.33	13.48	25.55

[a] Average value. [b] Coefficient of variation.

3.7. Microstructure Model of Pre-oxidized Fibers

According to the above research results, the internal microstructure of the pre-oxidized fiber was analyzed, the structural morphology of the pre-oxidized fiber was summarized, and the microstructure model of the pre-oxidized fiber was established, as shown in Figure 8.

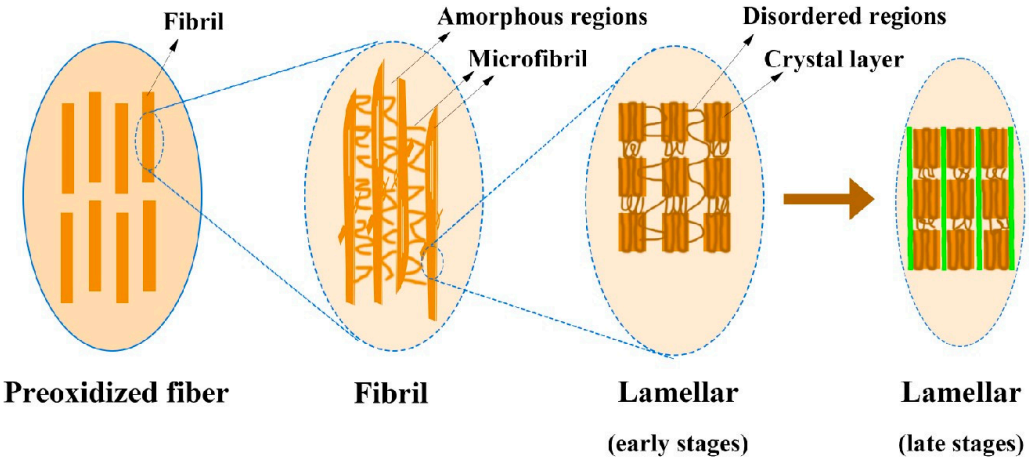

Figure 8. Microstructure model of pre-oxidized fiber.

The surface of the pre-oxidized fibers was smooth and compact, and the interior was composed of fibrils, which were formed by the aggregation of microfibrils of different sizes, including transverse microfibrils and longitudinal microfibrils. The longitudinal microfibrils were connected through transverse microfibrils and amorphous regions.

The lamellar structure in the protofilament was inherited inside the pre-oxidized fibers. Microfibrils are composed of lamellae stacked along the fiber axis, in which ordered crystal

layers and disordered regions are arranged alternately, and disordered regions are etched away by a DMSO solution during dissolution etching.

In the pre-oxidation stage, the fiber underwent chemical reactions, the linear molecular chain began to transform into a ring structure, and a ring structure began to form inside the lamella. As pre-oxidation progressed, the chemical reactions became intense, and a large number of ring structures were generated. The ring structures were cross-linked to form a trapezoidal structure. The solvent corrosion resistance of pre-oxidized fibers was constantly improved, and only part of the region was dissolved during solution etching. During the late pre-oxidation stage, the trapezoidal structure was arranged in an orderly manner around the lamella, and the connection between the primary fibers was enhanced. The fiber structure became more compact and stable. The pre-oxidized fibers and ultra-thin fiber slices were not easy to dissolve in the DMSO solution.

4. Conclusions

In this paper, pre-oxidized polyacrylonitrile-based carbon fibers were treated via ultrasonic etching and solution-etched ultrathin sections. The changes in fiber microstructures during the pre-oxidation process were studied; the pre-oxidation microstructure model was established and combined with the changes in its chemical structure. The FTIR results indicated that cyclization, oxidation, and dehydrogenation occurred during pre-oxidation. The XRD results showed that with the increase in temperature during the pre-oxidation process, the crystal size and crystallinity of the pre-oxidized fibers continuously decreased, the PAN linear molecular chain changed into a cross-linked trapezoidal structure, and the degree of cyclization increased. The SEM observations of the morphology and cross-section of the fibers after tensile fracture of the pre-oxidized fibers, following ultrasonic etching, showed that as pre-oxidation progressed, the fiber skin became denser, the corrosion resistance increased, and the fibers transitioned from ductile to brittle fracture. HRTEM observations of the ultrathin cross-sections of the fibers after solution etching indicated that the amorphous structure was dissolved, the original fiber structure was separated, and the longitudinal microfibers were connected by transverse microfibers and amorphous structures. The analysis results of fiber structure were summarized and a new model for the evolution of pre-oxidized fiber structure was proposed.

Author Contributions: Conceptualization, Y.S. and Y.W. (Yanxiang Wang); methodology, Y.S. and Y.W. (Yongbo Wang); software, B.D.; validation, Y.S.; formal analysis, J.G.; investigation, Y.S., Y.W. (Yanxiang Wang) and L.W.; resources, S.D. and Y.W. (Yuxia Wang); data curation, Y.S.; writing—original draft preparation, Y.S. and Y.W. (Yongbo Wang); writing—review and editing, Y.S. and Y.W. (Yanxiang Wang); visualization, Y.S.; supervision, Y.W. (Yanxiang Wang) and Y.W. (Yongbo Wang); project administration, Y.W. (Yanxiang Wang) and L.W. All authors have read and agreed to the published version of the manuscript.

Funding: This research was funded by the Natural Science Foundation of Shandong Province (ZR2021ME194, 2022TSGC2448, 2023TSGC0545), and the Key Technology Research and Development Program of Shandong Province (2021ZLGX01).

Data Availability Statement: The data that support the findings of this study are available upon request from the corresponding author, Yanxiang Wang, upon reasonable request.

Acknowledgments: The authors thank the editor and the anonymous reviewers for their valuable comments on this manuscript. The authors also acknowledge the support of technical staff for assisting in preparing samples and analyzing them.

Conflicts of Interest: The authors declare no conflicts of interest.

References

1. Liu, Y.; Kumar, S. Recent Progress in Fabrication, Structure, and Properties of Carbon Fibers. *Polym. Rev.* **2012**, *52*, 234–258. [CrossRef]
2. Frank, E.; Steudle, L.M.; Ingildeev, D.; Spörl, J.M.; Buchmeiser, M.R. Carbon Fibers: Precursor Systems, Processing, Structure, and Properties. *Angew. Chem. Int. Ed.* **2014**, *53*, 5262–5298. [CrossRef]

3. Ursache, Ș.; Cerbu, C.; Hadăr, A. Characteristics of Carbon and Kevlar Fibres, Their Composites and Structural Applications in Civil Engineering—A Review. *Polymers* **2024**, *16*, 127. [CrossRef]
4. Kim, K.-W.; Jeong, J.-S.; Chung, D.C.; An, K.-H.; Kim, B.-J. Effects of Surface Etching on Microstructure and Mechanical Strength of Carbon Fibers. *Carbon Lett.* **2018**, *28*, 100–104.
5. Yang, M.; Sun, L.; Liu, Q.; Deng, Y.; Liu, C.; Li, N.; Xu, J.; Chen, Y.; Jian, X. Ultra High Density Carbon Fiber Derived from Isotactic Polypropylene Fiber without Skin-Core Structure. *Polym. Adv. Technol.* **2024**, *35*, e6300. [CrossRef]
6. Jang, M.; Fliri, L.; Trogen, M.; Choi, D.; Han, J.-H.; Kim, J.; Kim, S.-K.; Lee, S.; Kim, S.-S.; Hummel, M. Accelerated Thermostabilization through Electron-Beam Irradiation for the Preparation of Cellulose-Derived Carbon Fibers. *Carbon* **2024**, *218*, 118759. [CrossRef]
7. Wang, S.; Bai, J.; Innocent, M.T.; Wang, Q.; Xiang, H.; Tang, J.; Zhu, M. Lignin-Based Carbon Fibers: Formation, Modification and Potential Applications. *Green Energy Environ.* **2022**, *7*, 578–605. [CrossRef]
8. Li, D.; Lu, C.; Hao, J.; Wang, H. A Comparative Analysis of Polyacrylonitrile-Based Carbon Fibers: (I) Microstructures. *New Carbon Mater.* **2020**, *35*, 793–801. [CrossRef]
9. Lee, J.-E.; Choi, J.; Jang, D.; Lee, S.; Kim, T.-H.; Lee, S. Processing-Controlled Radial Heterogeneous Structure of Carbon Fibers and Primary Factors Determining Their Mechanical Properties. *Carbon* **2023**, *206*, 16–25. [CrossRef]
10. Newcomb, B.A. Processing, Structure, and Properties of Carbon Fibers. *Compos. Part Appl. Sci. Manuf.* **2016**, *91*, 262–282. [CrossRef]
11. Chen, R.; Huang, W.; Li, Z.; Shi, Y.; Liu, L.-Z.; Li, D.; Lv, B. Furnace for In-Situ Characterization of the Preoxidation of Polyacrylonitrile (PAN) Fibers by Wide Angle X-Ray Scattering (WAXS). *Instrum. Sci. Technol.* **2021**, *50*, 321–333. [CrossRef]
12. Lu, J.; Li, W.; Kang, H.; Feng, L.; Xu, J.; Liu, R. Microstructure and Properties of Polyacrylonitrile Based Carbon Fibers. *Polym. Test.* **2020**, *81*, 106267. [CrossRef]
13. Ma, J.; Zheng, Z.; Tang, Y.; Nagashima, H.; Miyoshi, T. Chemical Reactions in Poly(Acrylonitrile-Co-Itaconic Acid) during Stabilization as Revealed by Solid-State NMR Spectroscopy and 13C Isotope Labeling. *Carbon* **2023**, *215*, 118432. [CrossRef]
14. Ko, T.-H. Influence of Continuous Stabilization on the Physical Properties and Microstructure of PAN-Based Carbon Fibers. *J. Appl. Polym. Sci.* **1991**, *42*, 1949–1957. [CrossRef]
15. Cui, Y.; Liu, L.; Song, L.; Li, S.; Wang, Y.; Shi, Y.; Wang, Y. In Situ Study and Improvement of the Temperature Increase and Isothermal Retention Stages in the Polyacrylonitrile (PAN) Fiber Pre-Oxidation Process. *Polymers* **2024**, *16*, 547. [CrossRef] [PubMed]
16. Rahaman, M.S.A.; Ismail, A.F.; Mustafa, A. A Review of Heat Treatment on Polyacrylonitrile Fiber. *Polym. Degrad. Stab.* **2007**, *92*, 1421–1432. [CrossRef]
17. Jäger, H.; Cherif, C.; Kirsten, M.; Behnisch, T.; Wolz, D.S.; Böhm, R.; Gude, M. Influence of Processing Parameters on the Properties of Carbon Fibres—An Overview: Einfluss Der Fertigungsparameter Auf Die Eigenschaften Der Kohlenstofffasern—Ein Überblick. *Mater. Werkst.* **2016**, *47*, 1044–1057. [CrossRef]
18. Nunna, S.; Naebe, M.; Hameed, N.; Fox, B.L.; Creighton, C. Evolution of Radial Heterogeneity in Polyacrylonitrile Fibres during Thermal Stabilization: An Overview. *Polym. Degrad. Stab.* **2017**, *136*, 20–30. [CrossRef]
19. Ko, T.; Ting, H.; Lin, C.; Chen, J. The Microstructure of Stabilized Fibers. *J. Appl. Polym. Sci.* **1988**, *35*, 863–874. [CrossRef]
20. Gao, Q.; Jing, M.; Zhao, S.; Wang, Y.; Qin, J.; Yu, M.; Wang, C. From Microfibrillar Network to Lamellae during the Coagulation Process of Polyacrylonitrile Fiber: Visualization of Intermediate Structure Evolution. *Macromolecules* **2020**, *53*, 8663–8673. [CrossRef]
21. He, J.; Chen, Q.; Zhu, H.; Wang, Y.; Malik, H.; Ma, B.; Wang, X.; Zhang, H.; Liu, Y.; Yu, J. Microstructural Evolution during Dry-Jet Wet Spinning Postprocessing from Coagulation Bath Fiber to High-Performance Polyacrylonitrile Precursor Fiber. *ACS Appl. Polym. Mater.* **2024**, *6*, 1781–1789. [CrossRef]
22. Marczak, E.; Marczak, P.; Sztajnowski, S.; Lipp-Symonowicz, B. Studies of Structural Changes in PAN Fibers with Various Initial Structures under the Influence of Thermal Treatment in Media. *Autex Res. J.* **2019**, *19*, 217–227. [CrossRef]
23. Rahman, M.M.; Demirel, T.; Tunçel, K.Ş.; Karacan, I. The Effect of the Ammonium Persulfate and a Multi-Step Annealing Approach during Thermal Stabilization of Polyacrylonitrile Multifilament Prior to Carbonization. *J. Mater. Sci.* **2021**, *56*, 14844–14865. [CrossRef]
24. Zhu, Y.; Wilding, M.A.; Mukhopadhyay, S.K. Estimation, Using Infrared Spectroscopy, of the Cyclization of Poly(Acrylonitrile) during the Stabilization Stage of Carbon Fibre Production. *J. Mater. Sci.* **1996**, *31*, 3831–3837. [CrossRef]
25. Ling, Z.; Diao, F.; Sheng, X.; Li, T.; Cai, R.; Wang, Y. Chemical Reaction and Phase Transformation Mechanism of Electrospun Iron (III) Acetylacetonate-Polyacrylonitrile Fibers during Pre-Oxidation Process. *Chem. Phys. Lett.* **2023**, *832*, 140866. [CrossRef]
26. Ge, Y.; Fu, Z.; Zhang, M.; Zhang, H. The Role of Structural Evolution of Polyacrylonitrile Fibers during Thermal Oxidative Stabilization on Mechanical Properties. *J. Appl. Polym. Sci.* **2021**, *138*, 49603. [CrossRef]
27. Zhou, H.; Zhu, J.; Wang, H.-L. Tuning of Structural/Functional Feature of Carbon Fibers: New Insights into the Stabilization of Polyacrylonitrile. *Polymer* **2023**, *282*, 126157. [CrossRef]
28. Study on the Structure Evolution and Temperature Zone Regulation Mechanism of Polyacrylonitrile Fibers during Pre-Oxidation Process | Iranian Polymer Journal. Available online: https://link.springer.com/article/10.1007/s13726-023-01214-4 (accessed on 15 March 2024).